



# Turning a linear geometry force-balance accelerometer to a broadband seismometer: design, modeling, and evaluation

Nikos Germenis · Georgios Dimitrakakis ·  
Efthimios Sokos · Pantelis Nikolakopoulos

Received: 9 November 2022 / Accepted: 25 October 2023 / Published online: 10 November 2023  
© The Author(s) 2023

**Abstract** A new, improved approach in the design of broadband seismometers is presented. The design results in the implementation of a high performance, low cost, and simple-to-operate instrument. The proposed seismometer is based on a modified accelerometer followed by a continuous time integrator for providing velocity voltage output. It has a broadband response, flat in velocity from 120 s to 75 Hz, high sensitivity 1200 V/(m/s), and 40  $V_{pp}$  differential

output range. The acceleration integration method provides high performance at low frequencies, with self-noise well below the New Low Noise Model at the range 80 s–16 Hz. The mechanical system provides a perfectly linear response of its displacement sensing system. Evaluation, classification, and noise determination of the presented instrument are performed in terms of direct experimental measurements, simulations, and calculations based on raw data from the proposed sensor and from a commercial product with approximately equivalent performance. Its technical features and performance specifications guarantee accurate sensing of local events, with maximum power at the frequency range of 5 to 10 Hz, but also make it ideal for the recording of distant tectonic activity, where extremely weak motions at long periods are expected. The whole design is robust, lightweight, and weatherproof, comprising in this way a useful tool to geoscientists.

## Highlights

- A broadband seismometer design based on a previously developed force-balance accelerometer.
- A broadband seismometer using a simple PD feedback closed loop control topology.
- A low-cost 120 s seismometer with very low noise levels.

N. Germenis · P. Nikolakopoulos  
Machine Design Laboratory, Dpt. of Mechanical  
Engineering & Aeronautics, University of Patras, Rion,  
Greece

P. Nikolakopoulos  
e-mail: pnikolakop@upatras.gr

N. Germenis (✉) · G. Dimitrakakis  
GEObit-Instruments, Aghion Saranta 13, 26222 Patras,  
Greece  
e-mail: ngermenis@geobit-instruments.com

E. Sokos  
Seismological Laboratory, Dpt. of Geology, University  
of Patras, 26504 Rion, Patras, Greece  
e-mail: esokos@upatras.gr

**Keywords** Broadband seismometer · Force  
balance · Capacitive transducer · 120 s seismometer

## 1 Introduction

A major part of seismic data recording requires sensing of very weak ground motion, e.g., when monitoring very weak or very distant earthquakes. In the latter case, small displacements (in the nanometer scale) occurring along extended time spans (> 100 s) have

to be accurately sensed and filtered out of the global background noise. This kind of recordings may be achieved only with very sensitive–very low noise sensors. Several broadband seismometer designs have been presented, e.g., Usher and Guralp 1978; Nordrgen and Nelson 2012; Habbak et al. 2016; and Koutsoukos and Melis 2005. High-quality instruments, usually based on rotational pendulum mechanisms (e.g., Knezlik et al. 2012) with big masses and proportional-integral-derivative (PID) control architecture or other more complicated configurations, are so far either too expensive to purchase or not at all developed for commercial distribution, while details about their inner structure are only scattered or completely inaccessible to the public (Ackerley 2014; Townsend 2014). The present paper attempts to partially fill this gap.

In this work a new, high-performance seismometer is presented. Based on state-of-the art electronic components and a robust, linear motion–linear response mechanism, it attains noise levels comparable to those of some of the most successful commercial products. The whole device is simple in its electromechanical and electronic structure and therefore reliable, lightweight, and easy to install and operate, comprising this way a very useful tool to geoscientists.

The proposed broadband seismometer is a combination of a high-performance seismic accelerometer, followed by a continuous time analog integrator. The accelerometer's operation is based on a proportional-derivative (PD) control architecture in contrast to the PID design, common to broadband sensor design so far. The mechanical system is based on a previously designed force-balance accelerometer (Germenis et al. 2022) that has been modified to comply with the noise and bandwidth requirements of very weak ground motion recording. The performance of the proposed seismometer has been extensively verified by measuring its critical specification values and by side-by-side comparative operation with a well-established commercial seismometer of similar characteristics.

In the following sections, the new instrument design is described in detail. Besides its inner configuration, its technical features, and its performance, are also described. In the *Design Architecture* paragraph, the topology of the closed loop control is analyzed, followed by the description of the mechanical and the electronic part of the sensor. Furthermore, the instrument's theoretical and experimental *Noise Performance* is calculated. The paper concludes with the

sensor's *Transfer Function* estimation, and the comparison with a reference seismometer, under real conditions, i.e., the two sensors' recordings for a teleseismic and a local event, is compared. The last section offers a *Specifications and Performance Summary* of the instrument, tabulated in comparison to the reference sensor's technical features.

## 2 General description

The proposed seismometer utilizes state-of-the art electronic components and employs some proper analog electronics design methods to achieve high performance with simpler overall electronic circuitry. The integral part of the commonly used PID feedback has been eliminated, instead, a very low noise continuous time analog integrator is used that integrates the acceleration electrical signal in continuous time to produce the desired velocity output. This combination outputs an analog seismic signal proportional to ground velocity, with a flat response range extending from 120 s to 75 Hz. To accurately control and set the instrument's sensitivity, an adjustable gain differential output amplifier follows the analog integrator. This is a simplified design that contains only two feedback paths (P, D) and makes the seismometer's corner frequency set and calibration much easier.

Its mechanical system is an evolution of a previously developed linear based geometry setup used for the implementation of a high-performance seismic accelerometer (Germenis et al. 2022). The instrument's total self-noise is lower than the New Low Noise Model (NLNM) (Peterson 1993) approximately between 80 s and 16 Hz. For achieving this fine performance, the mechanical system of the accelerometer had to be significantly modified compared to that in Germenis et al. 2022, with a much larger seismic mass, much lower spring stiffness, and a much wider conductive area of the capacitive displacement transducer's plates, yet the rest of the architecture principles, e.g., the linear motion geometry, remain unaltered.

An electronic continuous time analog integrator, followed by an adjustable gain output amplifier, was designed to receive the displacement sensor output signal (acceleration) and convert it to velocity. In general, common analog integrators inject significant low-frequency noise to the output signal due

to their high low-frequency gain. The electronic continuous time analog integrator, used for the purposes of the present work, was carefully designed to provide a self-noise level below NLNM down to at least 35 s, a feature that, accordingly, results to the high performance of the instrument in terms of total noise. The electronic circuit has been simplified to the highest possible degree so that only one adjustable gain amplifier is used in the feedback loop, which further reduces the instrument's electronic self-noise throughout its bandwidth.

A sine wave generator feeds the capacitor plates of the mechanical system with a 16 kHz, 30 V<sub>pp</sub> carrier signal, necessary for the displacement transducer to act as a capacitive variable voltage divider. This signal is directed to the plates of the transducer as two 15 V<sub>pp</sub> signals with 180° phase shift.

The electronic circuit is implemented on a high-density, multi-layer (printed circuit board) PCB board, which is mounted on the top of each mechanical spring-mass system. Three similar mechanical systems (one per axis) with their electronic boards on top are combined to form the broadband seismometer: two identical systems form the horizontal seismic elements (N and E components) and a third one, similar, but slightly different regarding its metal frame shape, stands as the vertical sensing element (Z component). In fact, the vertical component is a horizontal component, but rotated by 90° to let its seismic mass oscillate in the Z direction. The hardware is enclosed into a rugged and waterproof aluminum casing with stainless steel base plate.

With the seismic mass of each of the three sensors (93 g) appreciably smaller than what is typically encountered in sensors with similar performance (150–200 g), and with several parts made of aluminum (external case, sensor frame), the overall setup is remarkably lightweight (3.2 kg) and appropriate for projects where seismic stations must be deployed in large numbers.

The instrument has no recentering servos. The centering is done electronically during power on, with automatic adjustment of the voltage amplitude at the capacitor plates. Centering is also available on demand, by driving the center command line low. For this purpose, a microcontroller continuously monitors the mass position and sets the capacitor plate voltage

to a level such that the current mass position does not produce any offset voltage.

The cost of raw materials for the fabrication of the triaxial instrument remains below \$1 k making it suitable and financially meaningful for an industrial production line. Yet, it must be noted that the prototype developed for the present work is a result of countless hours of CAD design and simulations (electronic circuitry and mechanical parts), tests and failures and the several various parts (sensor frames and mass, outer shell and PCBs) were partially manufactured by selected partners and providers. In other words, the presented instrument is not easily reproduced by amateur engineers.

### 3 Design architecture

The presented broadband seismic sensor consists of two main parts: (i) the modified accelerometer mechanical spring-mass system along with the double electromagnetic force actuator (forcer) and (ii) the electronics board. The simplified block diagram of the seismic sensor is presented in Fig. 1. A horizontal seismic element is illustrated; however, it can operate as a vertical seismic element if rotated by 90° and with the proper adjustment of the rest position of the seismic mass (during the fabrication stage) in order to center between the two capacitor plates.

The mechanical system is firmly positioned in a hollow aluminum frame, which in turn is tightly anchored with screws on the steel base. The acceleration is applied to the frame along the axial direction of the sensing element (the direction of the first oscillation mode, see Fig. 2 in the next section) and causes a displacement of the mass relative to the frame, which is sensed by the capacitance transducer with a sensitivity  $A_t$  [V/m]. The transducer's output voltage, at frequency  $f_c = 16$  kHz, is fed to a low noise preamplifier with gain  $A_1$ . The demodulator derives the seismic signal from the amplitude modulated carrier signal. The carrier signal, generated by the signal generator "osc," is a sinusoidal signal with amplitude 30 V<sub>pp</sub> and frequency  $f_c$ .

Amplifier  $A_2$  on the open loop path is the only trimmable amplification stage in the loop. Its output signal, converted to a current signal by an RC network (components  $C_d$ ,  $R_d$ , and  $R_p$ ) that implements a

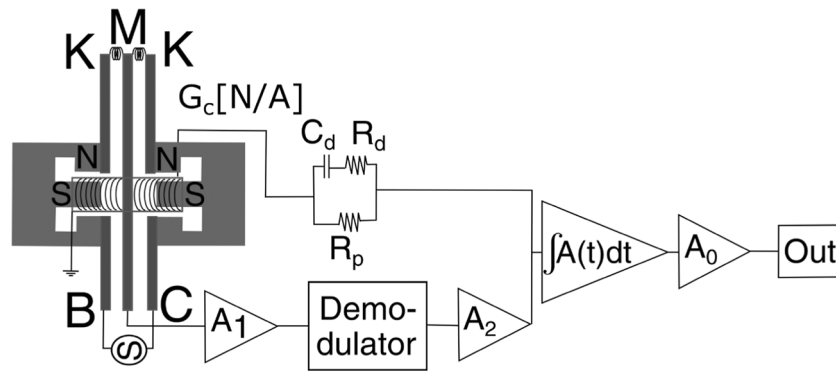


**Fig. 1** Seismic sensor, horizontal component simplified block diagram. *B*, *C* are the capacitor plates; *M* is the central plate (seismic mass); *N*, *S* are the North-South poles of the magnetic field generated by the double electromagnet along with the magnetic coil (showed as helical line) with  $G_c$  the force gener-

ator constant; and *K* is the spring constant.  $A_1$  is the VHF pre-amplifier,  $A_2$  is the open loop amplifier,  $\int A(t)dt$  is the integrator of any input signal  $A(t)$ , and  $A_0$  is the output amplifier.  $C_d$  and  $R_d$  are the resistor and capacitor of the derivative feedback path, and  $R_p$  is the resistor of the proportional feedback path

PD control logic, is fed to the “double” electromagnetic force actuator, which applies a restoring force to the seismic mass with a proportionality constant  $G_c$  [N/A]. The term “double” denotes that there are two coils on the seismic mass, electrically connected in series, interacting with two permanent magnets placed on both inner sides of the metal frame, as illustrated in Fig. 1. The output of  $A_2$  represents the acceleration signal, and it is driven to the analog integrator  $\int A(t)dt$  to obtain the velocity equivalent seismic signal. Unit  $A_0$  is the final output amplifier.

#### 4 Mechanical system: seismic mass and suspension

The seismic mass suspension design of the broadband seismic sensor is based on the linear geometry architecture of the force-balance accelerometer as presented in Germeis et al. 2022. Yet, this mechanical system has been subjected to some essential modifications: (i) The seismic mass has been significantly increased to 93 g, and (ii) the spring constant  $K$  has been decreased nearly ten times down to  $K = 130$ .

The seismic mass of a sensitive seismometer should not drop below a threshold value to ensure a mechanical system with self-noise lower than the NLNM at both the low-frequency and high-frequency ranges of the instrument’s bandwidth. The Brownian motion of the air molecules is a considerable noise source for the seismic mass and affects the overall

noise performance of the seismic sensor. In Riedesel et al. 1990, it has been demonstrated that the sensitivity of a light mass seismic sensor, exposed to air molecules, is by default limited because of this type of noise. The Brownian motion produces a noise equivalent acceleration  $a_B$  (Usher et al. 1977):

$$aB^2 = \frac{4Bk_B T \Delta f}{M^2} = \frac{4k_B T}{M} \frac{\omega_0}{Q} \left[ (\text{m/sec}^2)^2 / \text{Hz} \right] \quad (1)$$

where  $k_B = 1.38 \times 10^{-23}$  J/K is the Boltzmann constant,  $T$  is the absolute temperature [K],  $M$  is the seismic mass [kg],  $B$  is the viscous friction coefficient [ $\text{Nm}^{-1}\text{s}$ ], and  $Q$  is the quality factor of the spring-mass mechanism ( $Q = 1/2 \zeta$ , with  $\zeta = 4.2 \times 10^{-3}$  the damping factor of the present spring-mass system). Considering the condition  $\alpha_B^2 < 10^{-19}$  in a bandwidth of 1 Hz, for a spring-mass system with a power spectral density (PSD) of the Brownian equivalent acceleration lower than NLNM, the seismic mass must be at least 40 g if  $Q = 50$  and 10 g if  $Q = 100$ . However, if the condition for this theoretical minimum is satisfied, the actual seismic mass to be adopted in the design will depend on the performance of the closed control and output electronic circuits. A key feature of the proposed sensor that allows a seismic mass as small as 93 g is the fine, low noise performance of its electronic part.

In the proposed design, the seismic mass is suspended by a double leaf spring, thus creating an oscillating system with natural frequency  $f_0 = 6.1$  Hz and

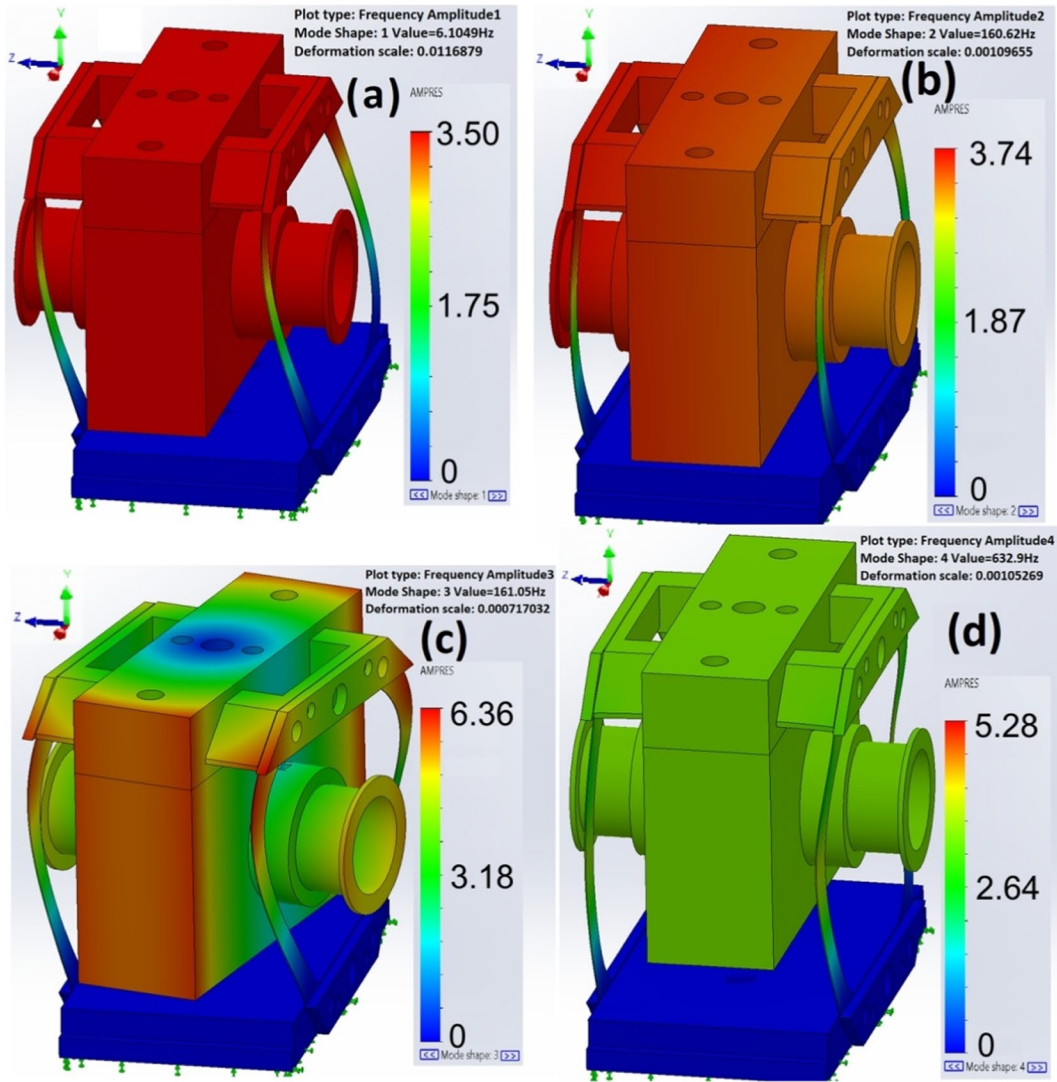


**Fig. 2** Illustration of the fundamental (a) and the first three higher oscillation modes (b, c, and d) of the mass-spring system: **a** Linear across simulation axis Z, 6.1 Hz. **b** Linear across simulation axis X, 160.6 Hz. **c** Rotational on simulation axis Y, 161 Hz. **d** Linear across axis Y, 632.9 Hz. The three arrows Z

(blue), Y (green), and X (red) show the simulation axes. For a horizontal component of the instrument, as in Fig. 1, the simulation axes X and Z define the horizontal plane. The displacement in the color scale is expressed in mm

$Q = 119$ . According to (1), it has an acceleration PSD  $\alpha_B^2 = 5.1 \times 10^{-20} \text{ (m/sec}^2\text{)}^2\text{/Hz}$ , which is lower than the acceleration power density of the NLNM model.

The modified mechanical system (the double spring and the mass with the attached force actuator coils) has been carefully designed and extensively simulated with finite element analysis (FEA) to ensure that only the fundamental oscillation mode frequency is in the recording band and any other

oscillation mode frequencies are outside of it. Several shapes and several spring material types were tested. For the springs, a standard mesh with high mesh density was selected, since this is the critical part of the mechanical system that gets deformed, and a typical coarse mesh was selected for the other items. Given the mass  $M$ , the spring’s material type and geometrical parameters determine all the oscillation modes.

Finite elements analysis investigation prior to fabrication included several simulations, and the outcome of this work indicated that the optimal performance is obtained with elliptical shape springs, properly processed to increase their elastic modulus. The material used is a stainless steel alloy, typically used for transformer laminations and the exact spring shape results from that adopted in Germenis et al. 2022, but with proper extraction of material from the leaf's profile in order to reduce its stiffness, yet with care taken for the new weaker design to withstand the 93 g of the seismic mass without any flexion and without the introduction of new natural eigenfrequencies in the band of interest (below 75 Hz). The result was a spring-mass system with its fundamental free oscillation frequency at  $f_o = 6.1$  Hz and with the next three oscillation mode frequencies at 160.6 Hz, 161 Hz, and 633 Hz (Fig. 2), all of them far outside the desired recording band of the sensor (120 s–75 Hz). The several mesh creation options allow an approximate  $\pm 1\%$  error at these results. A simple free oscillation test verified the match of the actual  $f_o$  with that predicted by the FEA software.

## 5 Electronic system

### 5.1 Signal generator

A typical automatic gain control Wien bridge signal generator, followed by a differential amplifier, is used to drive a 1:9 center tapped audio transformer. The secondary transformer coils produce two out of phase  $15 V_{pp}$ ,  $f_c = 16$  kHz sinusoidal signals, which drive the variable capacitor stationary plates on the mechanical system. The transformer center tap is grounded.

### 5.2 Capacitive displacement transducer

The capacitive transducer, which is formed by the two stationary conductive plates B and C and the central moving plate, senses accurately in continuous time the position of the seismic mass  $M$ . The output voltage of the capacitive transducer is (Germenis et al. 2022)

$$V_d = \frac{V}{2} \cdot \frac{x}{d} \quad (2)$$

where  $V$  is the amplitude of the carrier signal,  $x$  is the displacement of the mass from its rest position, and  $d$  is the distance between adjacent plates at rest. It is obvious that an increase in the capacitive transducer output voltage will result in a lower-level amplification necessary in the open loop path, so the mass plate mechanical system is built with  $d_1 = d_2 = d = 0.2$  mm at rest position, and the applied voltage  $V$  across the capacitor plates B and C is  $30 V_{pp}$ .

### 5.3 Displacement transducer sense circuit

As already mentioned, the displacement transducer is formed by the capacitor plates B and C and the central capacitor plate, which is the seismic mass (Fig. 1). The seismic mass is made of bronze (conductive), and therefore it may stand as the central capacitor plate. The induced voltage can be driven to the input of  $A_1$  with the use of very thin 44 AWG enameled copper wire soldered on it.

For the amplification of the displacement transducer output voltage, a dual stage preamplifier is used ( $A_1$  in Fig. 1). This unit is a high impedance audio amplifier implemented with two field effect transistors in cascode mode, followed by a differential output operational amplifier (follower) that feeds the demodulator stage with the in-phase and the out-of-phase signals. The combination of the cascode amplifier and the follower provides a very high impedance amplifier, which can be assumed as ideal, for the purposes of the present analysis. The sensitivity of this stage (displacement transducer plus  $A_1$ ) was measured at  $2.3 \times 10^5$  V/m. With the applied voltage amplitude being fixed, this result depends on three parameters: the distance  $d$  between the plates at rest position as in (2), the area  $A$  of the plates (here  $A = 676$  mm<sup>2</sup>), and the overall extra gain of the preamplifier  $A_1$ . The capacitive transducer operates linearly at nearly all the travel distance of the seismic mass due to its linear architecture.

### 5.4 Demodulator and signal amplifier

The demodulator is implemented with a dual complementary metal–oxide–semiconductor switch integrated circuit. It receives the modulated signal as an in-phase and an out-of-phase component from the differential amplifier that follows the preamplifier  $A_1$  and demodulates it operating at switching frequency  $f_c$ ,

synchronized by a zero-crossing detector circuit. The switches are followed by a signal amplifier ( $A_2$ ) that implements a single pole low-pass filter with cutoff frequency 150 Hz. This low-pass filter is used to filter out the carrier signal from the seismic signal, and the specific amplifier is the only gain adjustable signal amplifier inside the whole closed loop.

### 5.5 Feedback control

The feedback network consists of only three passive elements ( $R_d$ ,  $C_d$ , and  $R_p$  in Fig. 1) and controls the feedback current to the force actuator coils. The proportional path of the feedback is controlled by  $R_p$  (damping control) and the derivative path by  $R_d$  and  $C_d$  (overshoot control). The values of these elements are carefully selected to provide approximately critical damping with negligible overshoot (lower than 5%). The force transducer is a combination of a double coil–magnet set, electrically connected in series, and has a generator constant equal to  $G_c = 19$  N/A. The result of the feedback control to the mechanical system is to provide a force-balance acceleration sensor with flat response from 0 to 75 Hz.

### 5.6 Integrator

The integrator is implemented using a low noise operational amplifier (90 nV<sub>pp</sub> between 0.1 and 1 Hz), with 4.4 nV/ $\sqrt{\text{Hz}}$  input noise voltage density at 10 Hz and 20 nA input bias current. The integrator constant is  $R_t C_t = 120$  s. A feedback network (R network) is used to increase stability and eliminate any offset voltage. The integrator topology is illustrated in Fig. 3.

### 5.7 Assembly

The three seismic sensing elements (N, E, Z directions) are mounted on a stainless steel base (Fig. 4). Thin aluminum sheets that have been placed between the seismic elements act as screening of the electromagnetic interference (EMI) produced by each of them from the high-voltage–high-frequency carrier signal. Additional EMI suppression has been achieved by shielding the audio transformers of each seismic element. The seismic and control signals are connected with 1-mm pitch wire assemblies to the seismometer’s mainboard, which

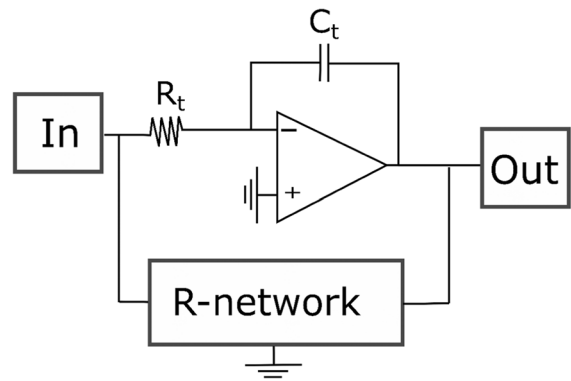


**Fig. 3** Integrator topology. “In” and “Out” represent the input and output signals, respectively; “R network” is the integrator feedback resistive network. The components  $R_t$  and  $C_t$  define with their product the integration constant ( $R_t C_t$ )

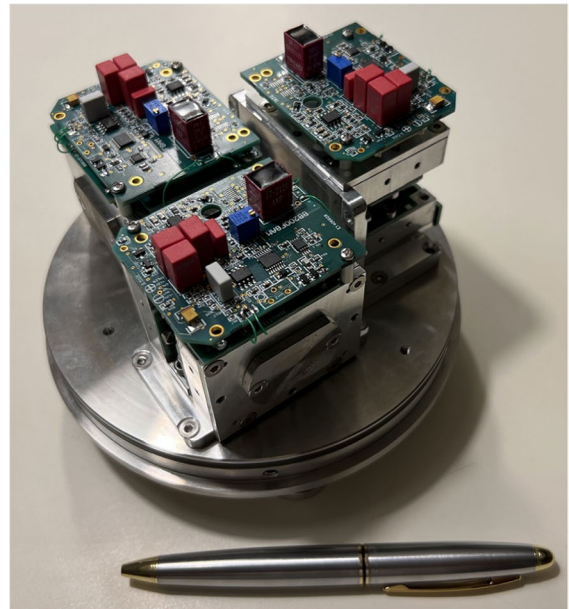


**Fig. 4** All three sensors of the instrument, assembled on the metal base

is located below the cover lid. The lid and the outer shell cylinder are made of high-density aluminum alloy. The metallic casing, further than 100% waterproof, also provides additional EMI shielding to the seismometer’s electronics.

## 6 Noise performance

### 6.1 Noise floor estimation

The self-noise determination of a sensitive seismological instrument involves some substantial difficulties (Barzilai et al. 1998). Brownian motion of the air surrounding the sensor, analyzed above, is one problem. Yet, the most important effect that distorts any self-noise measurements is the globally present background noise, which is mainly due to wave energy release across all the coastal lines of the planet (Peterson 1993). The proposed seismometer's self-noise has been determined using three different methods. Each of them provided a slightly different result from the other two, yet the differences can be fully justified.

### 6.2 Method 1: theoretical electronic circuit self-noise estimation

The first method applied was an electronic circuit noise prediction using the LTspice software (Analog

Devices 2022). The analog electronic circuit of the seismometer (Fig. 1) was analyzed with all the resistors, capacitors, and operational amplifiers selected to match those used in the real electronic board. The mechanical system (mass, springs, forcer) was not considered during this noise analysis. The result has been converted to  $(\text{m/sec})^2/\text{Hz}$  (dB), and it is plotted with a blue-colored line in Fig. 5 (“Theoretical Electronics”). It is evident that the theoretical electronic circuit analysis indicates very low noise levels in the range of high frequencies. Low-frequency noise is mainly due to the integrator. In Fig. 5, Peterson's NLNM and New High Noise Model (NHNM) in velocity units are also included for reference.

### 6.3 Method 2: electronic circuit self-noise measurement

The second method was to measure the electronic circuit noise at the absence of the mechanical system. The capacitive transducer's plates were replaced by two equal capacitors in series with the signal

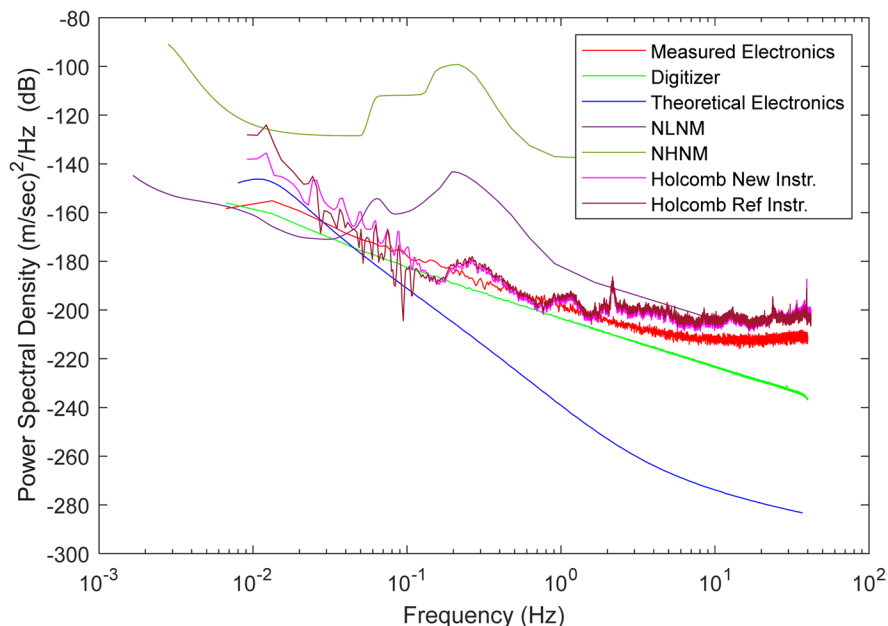


**Fig. 5** Self-noise estimation represented as power spectral density plots calculated with three different methods. “Measured Electronics” is the electronics (sensor + digitizer) self-noise measurement, “Digitizer” is the external connected digitizer self-noise, “Theoretical Electronics” is the theoretical self-noise of the sensor’s electronics calculated from the

LTspice simulation software, “Holcomb New Instr.” is the self-noise of the proposed instrument, and “Holcomb Ref Instr.” that of the reference instrument as they are calculated using the Holcomb method. “NLNM,” “NHNM” are the boundaries of the new noise model in velocity units as defined by Peterson



generator “osc” (Fig. 1), and the common pin was connected to the analog preamplifier of the circuit. With this configuration, the seismometer operation could be simulated in a condition of a completely stationary seismic mass. The noise analysis result from this experiment is plotted with the red line in Fig. 5 (“Measured Electronics”).

It is apparent that the self-noise estimations of the two methods (method 1 and method 2) have very good coincidence in the low-frequency range but a big difference, of more than 60 dB, at high frequencies. This result leads to the logical assumption that the cause of this difference is the self-noise of the digitizer used to implement the second method (GEObit’s GEOSix model was used). Thus, the digitizer self-noise plot is also included in Fig. 5 (green line, “Digitizer”). The digitizer noise level is the limit that does not allow measurement of noise levels below that, and in accordance with this fact, it was not possible to detect noise levels as those indicated by the theoretical simulations for the analog electronic circuit of the sensor. Indeed, the measured electronic noise has quite similar spectral profile with the digitizer’s noise, which proves that the noise measurement of method 2 is limited by the digitizer’s noise level.

#### 6.4 Method 3: self-noise estimation using another broadband seismometer

This method has been introduced in Holcomb 1989 (also applied in Tasič and Runovc 2012). For its application, two similar (in terms of self-noise) seismometers, both with unknown self-noise levels, are required to operate side-by-side. The proposed broadband seismometer and a co-located reference instrument (Nanometrics Inc. 2022; Xu and Yuan 2019) were left to record data into a six-channel datalogger (GEOSix). A relatively quiet segment of data (quiet in terms of actual seismic activity) was selected for further process. The input for the analysis is the two signals, and intermediate output is their spectral densities, their cross spectral density, and their squared coherence as functions of frequency, all calculated here with MATLAB (MathWorks 2022). The plot of the squared coherence of the two signals is shown in Fig. 6. The final result, i.e., the self-noise calculation of the proposed sensor, is plotted in Fig. 5 with magenta line (“Holcomb New Instr”), while the self-noise calculation of the reference sensor

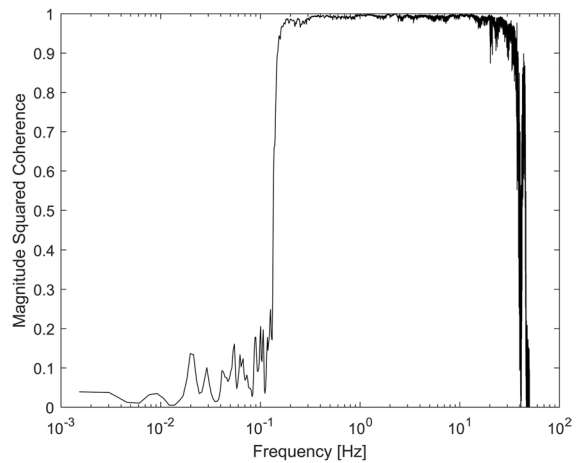


**Fig. 6** Squared coherence of the signals acquired from the proposed sensor and the reference broadband seismometer

is plotted with brown line (“Holcomb Ref Instr.”). The main principle of the approach is based on the idea that similar (highly coherent) signals constitute actual ground vibrations recorded from both sensors and loosely coherent signals indicate self-noise. As expected, with the sensor free to move under the effect of external causes (e.g., Brownian air motion and sounds), the noise levels at high frequencies (> 1 Hz) are slightly higher than those of the stationary plate measurement.

### 7 Transfer function

The transfer function of a seismometer is of crucial importance for the in-depth understanding of its performance, considering bandwidth sensitivity and stability. This information is necessary for the recorded raw data to be converted to actual seismic recordings.

In the direction of deriving the instrument’s transfer function, the transfer functions of its several discrete parts should first be known. These functions are listed below. For the mechanical part, it is

$$F_m(s) = [s^2 + (B/M)s + (K/M)] - 1 \tag{3}$$

where  $s = j\omega$  is the complex frequency in the frequency domain and  $K$  is the spring stiffness [N/m]. For the feedback branch, it is

$$F_f(s) = (k_1s + 1)/(k_2s^2 + k_3s + k_4) \tag{4}$$

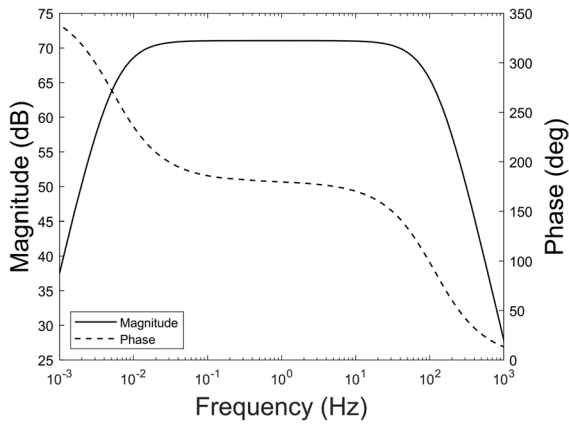


**Fig. 7** Plot of the proposed seismometer’s magnitude and phase response

where the coefficients  $k_1-k_4$ , related to the electrical parameters of the feedback branch, are known quantities. Finally, for the output integrator, it is

$$F_{oi}(s) = -s / (s + \omega_{oi})^2 = -s / (s^2 + 2\omega_{oi}s + \omega_{oi}^2) \quad (5)$$

with  $f_{oi} = \omega_{oi} / 2\pi = 8.33 \text{ mHz} = 1/120 \text{ s}$ .

Considering all the electronic circuit and mechanical part design parameters of the proposed seismometer, by combination of the expressions (3), (4), and (5), its transfer function turns out to be a ratio of polynomials:

$$G(s) = \frac{\sum_{k=0}^m a_k s^k}{\sum_{\lambda=0}^n b_\lambda s^\lambda} = \frac{a_5 s^5 + a_4 s^4 + \dots + a_0}{b_7 s^7 + b_6 s^6 + \dots + b_0} \quad m = 5, n = 7 \quad (6)$$

with the coefficients  $a_k, b_\lambda$  being precisely determined. With the use of MATLAB software (curve fitting tool) and without loss of precision, this expression is approximated with a simpler one, which serves as the final transfer function:

$$G(s) = \frac{-6.5 \times 10^8 s^2}{s^4 + 1460s^3 + 5.33 \times 10^5 s^2 + 3.52 \times 10^4 s + 580.3} \quad (7)$$

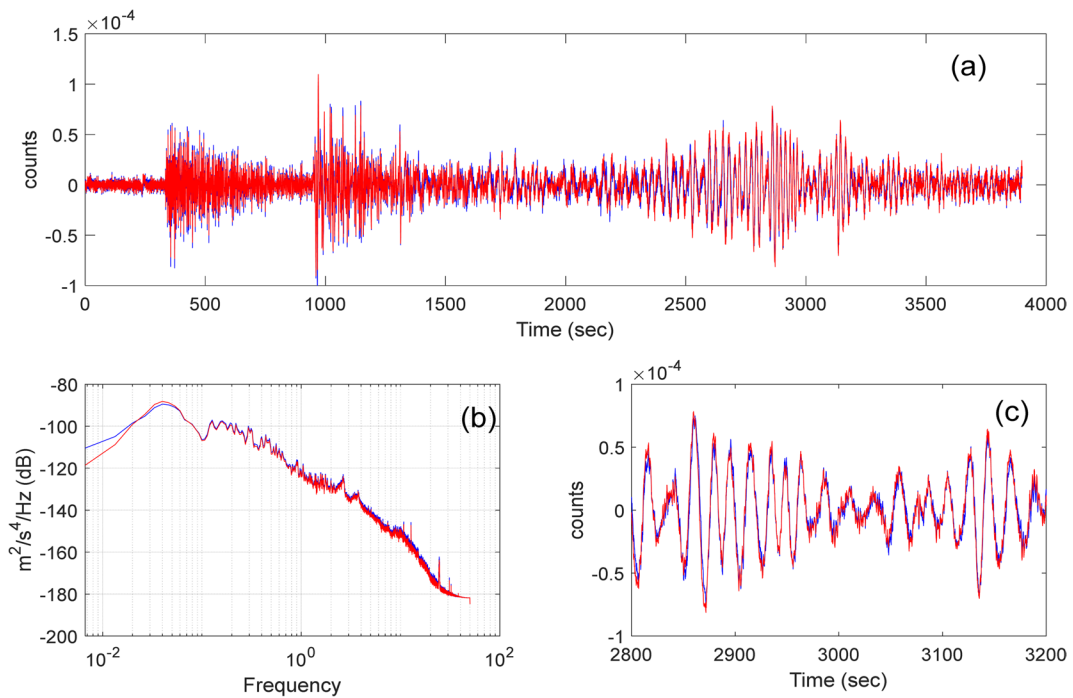


**Fig. 8 a** Teleseism record of an earthquake in Japan (7.1 Mw, Feb. 13, 2021) at distance 10.000km, as recorded by the proposed sensor (red line) and the reference sensor (blue line),

**b** overall signal PSD comparison, and **c** zoom in the surface wave arrival time window

The Bode plot (magnitude and phase) of this transfer function is illustrated in Fig. 7. It has a double zero at 0 Hz and two double poles at 5.3 mHz and 116.2 Hz. The cutoff frequencies are 8.15 mHz (123 s) and 75 Hz.

### 8 Seismometer earthquake recordings

The seismometer has been evaluated extensively at the University of Patras, Greece, Seismological Laboratory seismic pier. During the evaluation period, the seismometer recorded some teleseismic events and many local and regional earthquakes. We analyze a teleseism that occurred on Feb. 13, 2021, in Fukushima, Japan, having a magnitude 7.1  $M_w$ , and a local earthquake of magnitude 2.7  $M_w$  that occurred on Sept. 30, 2022, at an epicentral distance of 110 km. The PSD analysis of the earthquake recordings of the new broadband seismometer and the reference seismometer are illustrated in Figs. 8 and 9. The match

of the power density profiles for both events confirms equal performance of the proposed sensor with the reference one.

### 9 Specifications and performance summary

The specifications and performance of the proposed instrument are summarized in Table 1, tabulated along with the corresponding characteristics of the reference instrument mentioned in the previous sections.

### 10 Conclusions

In this work, a new broadband seismometer is presented, with flat response from 120 s to 75 Hz. The new sensor utilizes a linear displacement spring-mass mechanism

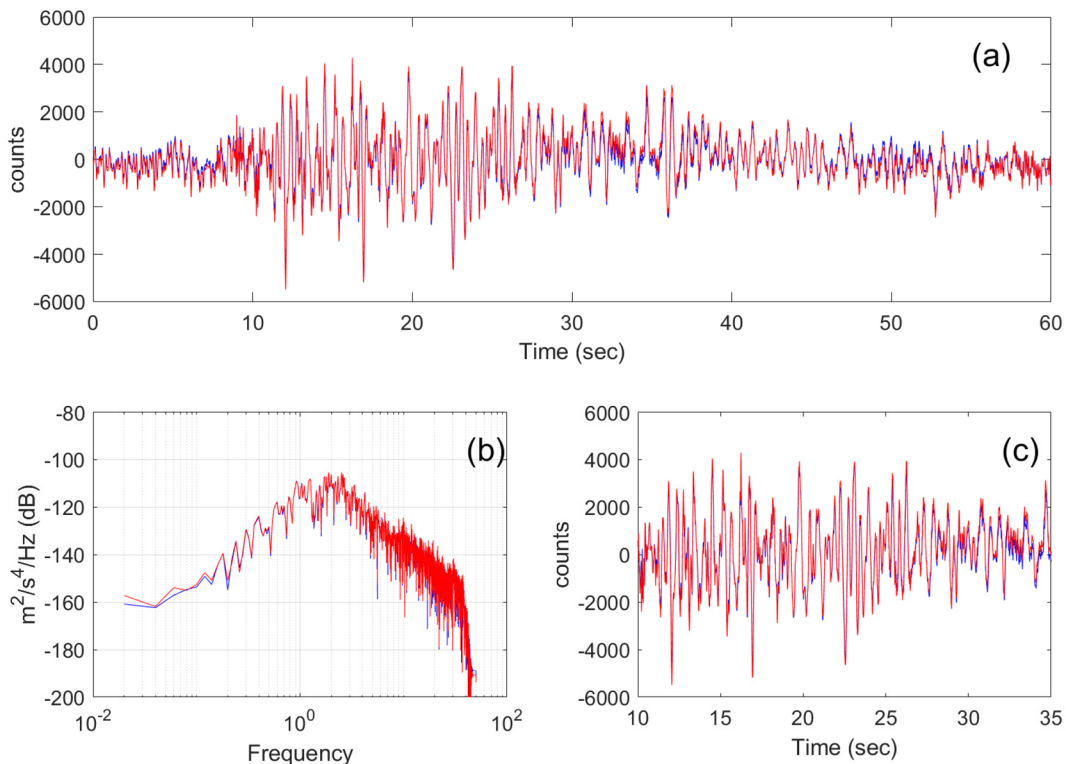


**Fig. 9** **a** Record of a local earthquake in Greece (2.7 Mw, Sept. 30, 2022) of epicentral distance 110 km as recorded by the proposed sensor (red) and the reference sensor (blue), **b** overall signal PSD comparison, and **c** zoom in the surface wave arrival time window

**Table 1** Comparison table between the new proposed instrument and the reference instrument (Trillium120PA)

Characteristic	New proposed instrument	Reference instrument
Flat response (Hz)	120 s–75 Hz	120 s–175 Hz
Range below NLNM (Hz)	80 s–16 Hz	35 s–10 Hz
Weight (kg)	3.2 kg	7.5 kg
Energy consumption	1 W	0.62 W
Sensor type	Force-balance with capacitive transducer	Force-balance with capacitive transducer
Centering	automatic	automatic
Mass lock	Not required	Not required
Mechanical system	Linear motion architecture	Pendulum architecture
Sensitivity	1200 V/m/s	1200 V/m/s

and adopts an electronic control circuit with very low noise components and a carefully designed integration unit. Simplified design architecture with PD feedback loop has been implemented instead of the commonly used PID architecture in many broadband sensors. These facts, besides the fine high-frequency features, allow high sensitivity and low noise performance at low frequencies with a relatively small seismic mass. The overall design is remarkably lightweight, robust, and reliable. The sensor's self-noise spectral profile is determined based on simulations, measurements, and calculations that indicate its excellent performance regarding noise levels.

**Author contributions** Nikos Germenis: Did the design, implementation, and testing of the instrument, wrote the manuscript.

Georgios Dimitrakakis: Did the modeling of the instrument and wrote parts of the manuscript.

Efthimios Sokos: Did the analysis of the recorder data, did some of the figures and reviewed the manuscript.

Pantelis Nikolakopoulos: Supervised the mechanical analysis and reviewed the manuscript.

**Funding** Open access funding provided by HEAL-Link Greece.

**Data availability** Data used in this study were acquired during the sensor evaluation. Detailed mechanical drawings, materials, and electronic circuit diagrams are proprietary. They cannot be released to the public.

## Declarations

**Ethics approval and consent to participate** Not applicable.

**Consent for publication** The authors consent for publication.

**Competing interests** The authors declare no conflict of interest.

**Open Access** This article is licensed under a Creative Commons Attribution 4.0 International License, which permits use, sharing, adaptation, distribution and reproduction in any medium or format, as long as you give appropriate credit to the original author(s) and the source, provide a link to the Creative Commons licence, and indicate if changes were made. The images or other third party material in this article are included in the article's Creative Commons licence, unless indicated otherwise in a credit line to the material. If material is not included in the article's Creative Commons licence and your intended use is not permitted by statutory regulation or exceeds the permitted use, you will need to obtain permission directly from the copyright holder. To view a copy of this licence, visit <http://creativecommons.org/licenses/by/4.0/>.

## References

- Ackerley N (2014) Principles of broadband seismometry. Encyclopedia Earthquake Eng. [https://doi.org/10.1007/978-3-642-36197-5\\_172-1](https://doi.org/10.1007/978-3-642-36197-5_172-1)
- Analog Devices (2022) LTspice, available at <https://www.analog.com> (last accessed Jan. 2023).
- Barzilai A, VanZandt T, Kenny T (1998) Technique for measurement of the noise of a sensor in the presence of large background signals. Rev Sci Instrum 69(7):2767–2772
- Germenis N, Dimitrakakis G, Sokos E, Nikolakopoulos P (2022) Design, modeling, and evaluation of a class-A tri-axial force-balance accelerometer of linear based geometry. Seismol Res Lett. <https://doi.org/10.1785/0220210102>
- Habbak E, Nofal H, Lofty E, El-Sabban S, Nossair Z (2016) Design and simulation of a vertical broadband seismometer. Arab J Geosci 9:408. <https://doi.org/10.1007/s12517-016-2422>
- Holcomb L (1989) A direct method for calculating instrument noise levels in side-by-side seismometer evaluations. U.S. Geological Survey, Open-File Rept, pp 89–214

- IRIS (2022) Incorporated research institutions for seismology, available at <https://www.iris.edu/> (last accessed Jan. 2023).
- Knezlik J, Kalab Z, Rambousky Z (2012) Adaptation of the S-5-S pendulum seismometer for measurement of rotational ground motion. *J. Seismol* 16:649–656. <https://doi.org/10.1007/s10950-012-9279-6>
- Koutsoukos E, Melis N (2005) A horizontal component broadband seismic sensor based on an inverted pendulum. *Bull Seismol Soc Am* 95(6)
- MathWorks (2022) Matlab, available at <https://www.mathworks.com/> (last accessed Jan. 2023). Available at <https://www.mathworks.com/> (last accessed Jan. 2023).
- Nanometrics Inc. (2022) Trillium 120s data sheet available at <https://www.nanometrics.ca/> (last accessed Jan. 2023).
- Nordrgen B. and D. Nelson (2012) Yuma-2 seismometer, available at <http://www.groundmotion.org/> (last accessed Jan. 2023).
- Peterson J (1993) Observation and modeling of seismic background noise. U.S Geol Survey Technical Rept 93-322:1–95
- Riedesel M, Moore R, Orcutt J (1990) Limits of sensitivity of inertial seismometers with velocity transducers and electronic amplifiers. *Bull Seismol Socf Am* 80:1725–1752
- Tasič I, Runovc F (2012) Seismometer self-noise estimation using a single reference instrument. *J Seismol* 16:183–194. <https://doi.org/10.1007/s10950-011-9257-4>
- Townsend B (2014) Symmetric triaxial seismometers. *Encyclopedia Earthquake Eng.* [https://doi.org/10.1007/978-3-642-36197-5\\_194-1](https://doi.org/10.1007/978-3-642-36197-5_194-1)
- Usher M, Buckner I, Burch R (1977) A miniature wideband horizontal-component feedback seismometer. *J Phys E: Sci Inst* 10:1253–1260
- Usher M, Guralp C (1978) The design of miniature wideband seismometers. *J Geophys* 48:281–292
- Xu W, Yuan S (2019) A case study of seismograph self-noise test from Trillium 120QA seismometer and Reftek 130 data logger. *J. Seismol* 23:1347–1355. <https://doi.org/10.1007/s10950-019-09872-9>

**Publisher's Note** Springer Nature remains neutral with regard to jurisdictional claims in published maps and institutional affiliations.